

Modeling the elastic properties of concrete composites: Experiment, differential effective medium theory, and numerical simulation

by

Z. Sun*, E.J. Garboczi, and S. P. Shah*****

***University of Louisville, Louisville, KY USA**

****Building and Fire Research Laboratory
National Institute of Standards and Technology
Gaithersburg, MD USA**

*****Northwestern University, Evanston, IL USA**

Reprinted from Cement & Concrete Composites, 29, pg.22-38, 2007.

NOTE: This paper is a contribution of the National Institute of Standards and Technology and is not subject to copyright.

NIST

National Institute of Standards and Technology
Technology Administration, U.S. Department of Commerce



Modeling the elastic properties of concrete composites: Experiment, differential effective medium theory, and numerical simulation

Zhihui Sun ^{a,*}, Edward J. Garboczi ^b, Surendra P. Shah ^c

^a Department of Civil and Environmental Engineering, University of Louisville, Louisville, KY 40217, USA

^b Materials and Construction Research Division, National Institute of Standards and Technology, Gaithersburg, MD, USA

^c Center for Advanced Cement-Based Materials, Civil Engineering Department, Northwestern University, Evanston, IL, USA

Received 22 March 2006; received in revised form 17 July 2006; accepted 20 July 2006

Available online 26 September 2006

Abstract

Concrete is a mixture of cement, water and aggregates. In terms of microstructure, besides the cement paste matrix and aggregate inclusions, there is a third phase, which is called the interfacial transition zone (ITZ), which forms due to the wall effect and can be thought of as a thin shell that randomly forms around each aggregate. Thus, concrete can be viewed as a bulk paste matrix containing composite inclusions. To compute the elastic properties of a concrete composite, a differential effective medium theory (D-EMT) is used in this study by assigning elastic moduli to corresponding bulk paste matrix, ITZ and aggregate. In this special D-EMT, each aggregate particle, surrounded by a shell of ITZ of uniform thickness and properties, is mapped onto an effective particle with uniform elastic moduli. The resulting simpler composite, with a bulk paste matrix, is then treated by the usual D-EMT. This study shows that to assure the accuracy of the D-EMT calculation, it is important to consider the increase in the water:cement mass ratio (w/c) of the ITZ and the corresponding decrease in w/c ratio of the bulk matrix. Because of this difference in w/c ratio, the contrast of elastic moduli between the ITZ and the bulk paste matrix needs to be considered as a function of hydration age. The Virtual Cement and Concrete Testing Laboratory (VCCTL) cement hydration module is used to simulate the microstructure of cement paste both inside and outside the ITZ. The redistribution of calcium hydroxide between ITZ and bulk paste regions can further affect the elastic contrast between ITZ and bulk paste. The elastic properties of these two regions are computed with a finite element technique and used as input into the D-EMT calculation. The D-EMT predictions of the elastic properties of concrete composites are compared with the results measured directly with a resonant frequency method on corresponding composites. This comparison shows that the D-EMT predictions agree well with experimental measurements of the elastic properties of a variety of concrete mixtures.

© 2006 Elsevier Ltd. All rights reserved.

Keywords: Microstructure; Interfacial transition zone; Numerical simulation; Differential effective medium theory; Dynamic elastic moduli

1. Introduction

The mechanical properties, including compressive and tensile strength and elastic moduli, of cement-based materials are of primary importance for their use as structural materials. The study presented in this paper will focus on the linear elastic properties, which are represented by the

dynamic Young's modulus and the dynamic shear modulus of mortar and concrete composites.

As a composite material, concrete is a mixture of cement paste with aggregate inclusions of various sizes. However, concrete is not just a two-phase composite. It has been found that the presence of the grains in the paste causes a thin layer of matrix material surrounding each inclusion to be more porous than the bulk of the surrounding cement paste matrix. This layer is called the interfacial transition zone (ITZ) [1–6]. Studies by other researchers showed that

* Corresponding author. Tel.: +1 502 852 4583; fax: +1 502 852 8851.
E-mail address: z.sun@louisville.edu (Z. Sun).

the ITZ between the paste matrix and aggregate phases played an important role in the properties of a concrete composite [7,8]. It was found that the ITZ has a layered structure, and it has a lower density than the bulk matrix and is more penetrable by fluids and gases [9]. Therefore, it is the ITZ that determines the overall permeability of the concrete [10]. Also, due to its complex structure, the ITZ appears to be the weakest region of the composite material when exposed to external loads [11]. It has been found by experiment that the elastic moduli of concrete are intimately related to the elastic moduli and volume fraction of the ITZ regions [12]. Thus, when modeling concrete properties based on microstructure, it is necessary to consider the concrete or mortar as a three-phase composite consisting of bulk paste matrix, ITZ, and aggregate inclusions [13]. The bulk paste matrix and the ITZ are not really uniform materials, however, but this paper will show how uniformity can be approximated.

Recently, Yang [14,15] proposed a double-inclusion model for a mortar composite. In that model, the spherical aggregate was assumed to be surrounded by a concentric layer of ITZ, all embedded in the cement paste matrix. The thickness and the mechanical properties of ITZ layers were obtained from regression analysis. It was concluded that the thickness of ITZ is between 20 μm and 40 μm , and the mechanical properties of ITZ are related to its thickness. Li et al. [16] presented a numerical method, in which the mesostructure of concrete was simulated and the finite element method was employed for the stress analysis in the concrete. An ITZ thickness of 50 μm was used. It was found that the moduli of a concrete composite was closely related to the thickness and elastic moduli of the ITZ. A four-phase sphere model was also proposed by Li et al. [17,18] to predict the elastic moduli of a concrete composite.

A microstructural model, called the hard core soft shell (HCSS) model, was proposed by Garboczi et al. [19–22] to study the microstructure, conductivity, and mechanical properties of concrete. This was an idealized model in that all the ITZ regions were of the same thickness, and uniform around each spherical aggregate. The model was extended from Christensen and Lo's three-phase sphere model for two-phase composite materials [23]. In the model, the properties of a spherical aggregate and its concentric ITZ layer were mapped onto an effective uniform particle, making a single, larger inclusion which has elastic properties equivalent to the original composite inclusion. The elastic properties of the entire composite were then calculated with a differential effective medium theory (D-EMT) by considering the bulk paste matrix and the effective inclusion particles [20,21]. The simulated results with D-EMT were compared successfully with a special finite element method (FEM) [24] in both 2D and 3D [21], with simple but varying composite inclusion particle size distributions. Excellent accuracy of the D-EMT was found.

Recently, Nadeau [25,26] has developed the most comprehensive model of concrete elastic moduli to date, where

he takes into consideration the gradient of properties in the ITZ. He also realizes that the higher water:cement mass ratio (w/c) found in the ITZ regions forces the value for the bulk paste w/c to be lower, reflecting this redistribution of cement. By requiring the total amount of cement in his microstructure to be that given by the mix design, he forces the conservation of total cement. Once the microstructure was set up, he used a form of self-consistent effective medium theory to compute overall elastic properties of concrete. Nadeau used literature data on the elastic properties of cement paste and mortar to both build and validate his theory.

This present paper attempts to improve on Nadeau's work by: (1) making accurate experimental measurements of elastic moduli for a wide range of mortars and concretes and a wide range of degrees of hydration that were directly chosen for this work [27], (2) using a differential effective medium theory, which is more suited to mortar and concrete microstructure than are self-consistent effective medium theories, and (3) direct simulation of the ITZ and bulk paste microstructure, including the redistribution of CH between these two regions and its computed effect on local elastic moduli, to help give insight into what is actually occurring in these regions during mixing and hydration.

2. Differential effective medium theory (D-EMT)

Concrete is a good example of a composite material in which the inclusions (rocks and sand) are surrounded by a thin shell of altered matrix material (ITZ) and embedded in the normal matrix material. If we associate the ITZ layer totally with the aggregate, we can think of concrete as consisting of a matrix material containing composite inclusions. Assigning each of these phases different linear elastic moduli results in a complicated effective elastic moduli problem. This problem has previously been approached in the linear, isotropic conductivity and elasticity cases [20,21] by the idea that each inclusion particle, surrounded by a shell of another phase, is mapped onto an effective particle of uniform elastic moduli. The resulting simpler composite, with a normal matrix but slightly larger inclusions, is then treated in usual differential effective medium theory [28,29]. If one takes the ITZ thickness to be zero, then this version of D-EMT reduces to the usual D-EMT for spherical particles.

In Nadeau's work [25,26], a self-consistent effective medium theory was used to generate overall predictions for mortar and concrete elastic moduli. We believe that the D-EMT is better suited for concrete than are self-consistent effective medium theories, because it better matches the actual concrete microstructure consisting of generally non-touching aggregates in a cement paste matrix. The self-consistent theories can give artificial phase percolation effects for the inclusions that are just not present in concrete. In D-EMT, the only percolation threshold for inclusions is when the volume of fraction of inclusions is unity, which is never approached for real mortars and concretes.

This is true even for the slightly larger, effective particles found in this paper's version of D-EMT. It is thought that the ITZ regions do percolate and become continuous, but this has only a small effect on the overall elastic moduli. ITZ percolation has a much larger effect on transport [19,30–33] and perhaps crack propagation.

In concrete, the composite problem is even more complicated. The ITZ "shell" around each inclusion actually contains a gradient of properties, since the cement paste matrix density is least at the aggregate surface and increases outwards to the bulk paste density [1–4,19]. The inclusions in concrete are modeled as spheres, which is a good approximation for many concrete mixtures, especially when the elastic contrast between aggregate and paste is less than about five, when the shape of the inclusion is not so important [34–37]. Then, the dilute limit, which has a very small volume concentration of spherical inclusions surrounded by a thin layer containing a spherically symmetric gradient of point-wise isotropic elastic properties, can be handled exactly [38–41]. But the non-dilute microstructure of concrete, with a wide particle size distribution of inclusions, each surrounded by overlapping gradients of properties, is very difficult to treat analytically, by numerical methods, or by effective medium theory (EMT). In addition, since there is a nominal w/c ratio for the entire concrete, having a higher value of w/c in the ITZ, since there is less cement there, implies that there is a lower w/c value in the bulk paste, which is the paste outside the ITZ regions. For the conductivity case, it has been shown that a multi-scale model can be used in order to map this complex microstructure into a simpler microstructure in which the shell layers can be treated theoretically as having uniform properties [30–33]. Section 4 shows how a similar procedure can be carried out for the elastic case. The three-phase composite described above then becomes appropriate for the concrete elastic moduli problem.

3. Materials and experiments

3.1. Raw materials

Ordinary Type I Portland cement provided by Lafarge¹ was used for all experiments and simulations. The chemical phase compositions, obtained from a combination of scanning electron microscopy and X-ray microprobe measurement [42], are listed in Table 1 by volume fraction (%) of the cement. Their uncertainty is estimated to be ± 1 (%). The Blaine surface area was measured to be $365 \text{ m}^2/\text{kg}$, with an estimated uncertainty of $\pm 10 \text{ m}^2/\text{kg}$. The relative density was assumed to be 3.2.

¹ Certain commercial equipment and/or materials are identified in this report in order to adequately specify the experimental procedure. In no case does such identification imply recommendation or endorsement by the National Institute of Standards and Technology, nor does it imply that the equipment and/or materials used are necessarily the best available for the purpose.

Table 1
Chemical compositions of portland cement type I

Chemical Data	C ₃ S	C ₂ S	C ₃ A	C ₄ AF	Gypsum
Volume percent	72.6	4.8	10.1	5.5	7.0

A low angle laser light scattering (LALLS) method [43] was applied to measure the particle size distribution of the cement powder. Four tests were done and average values were used in the later numerical simulation work. It is important to note that 50% of the cement particles by mass had an equivalent spherical diameter smaller than $14 \mu\text{m}$, so that the median cement particle diameter was $14 \mu\text{m}$. Fig. 1 shows the results of this measurement in terms of a cumulative mass fraction plot.

River sand and naturally rounded coarse aggregate were used for casting mortar and concrete. The maximum diameter of the coarse aggregates was 12.5 mm. The grading of the aggregates complied with ASTM Standard C33-99a [44]. The cumulative particle size distributions of the sand and gravel are listed in detail in Table 2 (uncertainties of 0.1%), since this information is crucial for computing ITZ volume and for implementing the D-EMT. The relative density of the gravel was 2.62, and the relative density for the sand was 2.69.

3.2. Mix designs

Concrete or mortar with cement paste w/c ratios (mass ratio) ranging from 0.35 to 0.6 were used in both the experimental and the simulation research. The water-to-cement mass ratios, sand-to-cement mass ratios and the gravel-to-cement mass ratios that were used are listed in Table 3. Some bleeding was observed for the w/c = 0.5 and 0.6 pastes, but the layer of bleed water was re-absorbed by the paste after several hours, since the samples were sealed. No bleeding was observed for any of the mortar or concrete samples. The corresponding paste volume percentages compared to the total volume of each composite were also calculated and listed in the table. In Table 3, "c" represents

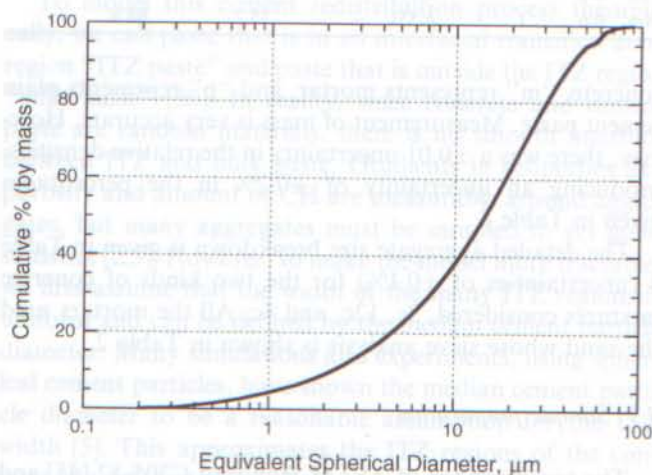


Fig. 1. Particle size distribution of cement (cumulative mass fraction).

Table 2
Sieve analysis of sand and gravel used for all mixtures

Sieve size (mm)	% Mass passing	Effective diameter (mm)	Mass fraction (%)
<i>Sand</i>			
9.5	100	7.12	1.0
4.75	99.0	4.38	1.5
4.0	97.5	3.68	1.8
3.35	95.7	2.86	5.7
2.36	90.0	2.18	2.5
2.0	87.5	1.85	3.0
1.7	84.5	1.35	9.8
1.0	74.7	0.8	16.2
0.6	58.4	0.46	24.4
0.32	34.0	0.22	29.2
0.12	4.78	0.097	1.29
0.074	3.49	0.037	3.49
0.0	0.0	0.0	0.0
<i>Gravel</i>			
12.5	100	11.0	3.8
9.5	96.2	7.14	61.1
4.75	35.1	4.05	21.7
3.35	13.4	2.86	9.22
2.36	4.18	2.18	0.78
2.0	3.4	1.85	0.48
1.7	2.92	0.85	2.92
0.0	0.0	0.0	0.0

Table 3
Mix design used in the experimental and simulation research

No.	Water	Cement	Sand	Gravel	Paste volume (%)	Aggregate volume (%)
1p	0.5	1	—	—	100	0
2m	0.5	1	2	—	52.4	47.7
3c	0.5	1	2	2	35.2	64.8
4c	0.5	1	2	2.5	32.5	67.5
5m	0.5	1	4.052	—	35.2	64.8
6p	0.35	1	—	—	100	0
7m	0.35	1	2	—	47.3	52.7
8m	0.35	1	2.5	—	41.8	58.2
9m	0.35	1	3.311	—	35.3	64.8
10p	0.6	1	—	—	100	0
11m	0.6	1	2	—	55.2	44.7
12c	0.6	1	2	2	37.9	62.2
13m	0.6	1	5.906	—	29.5	70.6
14m	0.6	1	4.551	—	35.2	64.8

concrete, "m" represents mortar, and "p" represents plain cement paste. Measurement of mass is very accurate. However, there was a ± 0.01 uncertainty in the relative densities, producing an uncertainty of $\pm 0.2\%$ in the percentages given in Table 3.

The detailed aggregate size breakdown is given in Table 4 (uncertainties of $\pm 0.1\%$) for the two kinds of concrete mixtures considered, 3c, 12c, and 4c. All the mortars used the sand whose sieve analysis is shown in Table 2.

3.3. Sample preparation

The specifications of ASTM-Standard C305-82 [45] and C192-88 [46] were followed during the mixing of paste,

Table 4
Combined sieve analysis for fine plus coarse aggregate for the two kinds of concrete mixtures considered

Diam (mm)	Concrete 3c, 12c mass fraction (%)	Concrete 4c mass fraction (%)
11.0	1.93	2.14
7.135	31.0	34.3
7.125	0.49	0.44
4.375	0.74	0.66
4.05	11.0	12.2
3.675	0.89	0.79
2.855	7.48	7.68
2.18	1.63	1.54
1.85	1.73	1.59
1.35	4.84	4.30
0.85	1.48	1.64
0.8	8.00	7.10
0.6	12.1	10.7
0.32	14.4	12.8
0.12	0.64	0.56
0.074	1.72	1.53

mortar and concrete, respectively. A saturated curing condition was used. The specimens were cast into the molds that were sealed and then submerged in a water bath, which was connected to a microprocessor controlled refrigerating/heating circulator. After 24 h, the molds were removed and the specimens were directly submerged in the water. The circulator continuously adjusted the temperature of the circulating water to the set value with an accuracy of ± 0.1 °C. A constant temperature of 25 °C was used throughout all the experiments.

3.4. Setting time test

Initial setting times of the plain cement pastes were determined by Vicat needle tests as specified by ASTM Standard C191-99 [47]. Needle settlements were read every 10 min. The means of the readings from three batches were used to define the initial and final setting time of each plain paste mixture. The measured initial setting times for plain pastes with $w/c = 0.35, 0.5,$ and 0.6 were 3.40 ± 0.69 h, 4.75 ± 0.41 h, and 6.25 ± 0.48 h, respectively (one standard deviation uncertainties from three samples). The curing temperature used was 25 °C. The measured setting times were used in the modeling of the properties of the ITZ and the bulk paste matrix, which will be presented below.

3.5. Dynamic moduli measurement

The resonant frequency method was adopted to determine the dynamic moduli of the cement paste, mortar, and concrete materials. Rectangular prism samples of size $(50 \pm 1) \text{ mm} \times (75 \pm 1) \text{ mm} \times (230 \pm 1) \text{ mm}$ were used. During the tests, one end of the sample was brought in contact with a contact type vibration generator and the other end was connected to a contact pick-up. Both the driver and the pick-up were connected to the E-meter, which in

turn was connected to an oscilloscope. By changing the frequency of the driver force, the reaction of the specimen was recorded. The frequency of the driver force at which the specimen has the maximum reaction is defined as the resonance frequency. By changing the location of the driver and pick-up, the resonance frequencies for the longitudinal and torsional vibration modes can be determined. According to ASTM-Standard C215 [48], dynamic Young's and shear moduli can be calculated from Eqs. (1) and (2) by measuring the resonance frequencies of the test specimens when vibrating in longitudinal and torsional modes, respectively:

$$E = B \cdot W \cdot (n')^2 \quad (1)$$

$$G = D \cdot W \cdot (n'')^2 \quad (2)$$

In these equations, E and G are the dynamic Young's and shear moduli, B and D are factors accounting for the shape and the size of the specimen, W is the mass of the specimen, and n' and n'' are the measured longitudinal and torsional resonance frequencies, respectively.

The measured dynamic Young's and shear moduli for mortar and concrete composites were used to inspect the accuracy of the D-EMT calculations presented in this paper. The experimental data for the dynamic moduli of the three cement pastes were used to help model the elastic properties of the ITZ and the bulk paste matrix of each concrete and mortar composite.

The dynamic moduli of the aggregates were determined with the ultrasonic pulse velocity method. The top and bottom parts of a large aggregate that was obtained by sieving were cut, and then ground until two parallel surfaces were obtained. The thicknesses of the aggregates were measured with a digital caliper and the measured wave velocities were used to determine the elastic moduli. In this study, the Young's modulus of the aggregate was determined to be 62.7 ± 5.0 GPa by assuming a Poisson's ratio of 0.2.

3.6. Thermogravimetric analysis (TGA)

Thermogravimetric analysis (TGA) was used to determine the degree of hydration of the pure cement pastes listed in Table 3 with hydration ages ranging from 2 h to about 60 d after mixing. In this experiment, the mass losses of the cement pastes at two different temperatures, 105 °C and 950 °C, were measured. The temperature was held at 105 °C for 2 h, and then was raised up to 950 °C with a rate of 10 °C/min. The evaporable and the non-evaporable water can be calculated through the mass measurement, and the degree of hydration values at each age can be determined with the Powers–Brownyard model [49] as shown in Eq. (3). The content of non-evaporable water for complete hydration $(w_n/c)_{\text{complete}}$ can be obtained from the Bogue potential composition [50] of the cement. A typical value for $(w_n/c)_{\text{complete}}$ is somewhere between 0.23 and 0.25. For the cement used in this study, a value of 0.247 was used. The loss on ignition was 0.0167 ± 0.0004 , which

was used to correct the degree of hydration measurements. In this research, it was assumed that the degree of hydration of mortars and concrete had the same average value as the corresponding cement paste. The uncertainty in the degree of hydration is dominated by the uncertainty in 0.247 value, since mass measurements are very precise. We estimate the uncertainty of each degree of hydration value to be ± 0.02 . The degree of hydration data were used to be able to match the hydration model, which gives degree of hydration directly but time indirectly, via an empirical fitting form:

$$\alpha(t) = \left[\frac{w_n(t)}{c} \right] / \left[\left(\frac{w_n}{c} \right)_{\text{complete}} \right] \quad (3)$$

4. Numerical simulation and modeling the properties of ITZ and bulk paste

4.1. Microstructure of concrete composite

We first introduce some theoretical ideas before discussing the numerical simulation of the ITZ microstructure and elastic properties. A real concrete is made up of aggregate particles having a wide size distribution and non-spherical shapes dispersed in a cement paste matrix. The cement paste matrix is a random collection of hydration products gluing together partially consumed, randomly shaped cement particles that are themselves made up of a random collection of mineral phases. From fundamental ideas about particle packing, it is clear that in the neighborhood of aggregate surfaces, on average there must be a smaller volume fraction of cement particles due to the wall effect [1–3,51]. This wall effect arises because particles cannot randomly pack as efficiently near a surface as in open space. However, the average w/c ratio of the paste is fixed. With less cement near aggregate surfaces, the w/c ratio is increased locally. This means that farther away from aggregate surfaces, the w/c ratio must be decreased in such a way that the overall value of the w/c remains at its nominal value [25,26,30,32].

To model this cement redistribution process theoretically, we call paste that is in an interfacial transition zone region "ITZ paste" and paste that is outside the ITZ region "bulk paste" [30]. In reality, since concrete and cement paste are random materials, there is no smooth interface between ITZ and bulk paste. Gradients in properties like porosity and amount of CH are measurable around aggregates, but many aggregates must be sampled to get good statistics [2,3]. However, to make the model more tractable, we first assume that the width of the many ITZ regions is uniform and can be defined by the median cement particle diameter. Many simulations and experiments, using spherical cement particles, have shown the median cement particle diameter to be a reasonable assumption for the ITZ width [5]. This approximates the ITZ regions of the concrete as a uniform width shell around each aggregate. Obviously there are effects farther out than a median cement

particle diameter, but the main effect on microstructure is within this region. Some ITZ regions clearly must overlap if two or more aggregate surfaces come within twice this length of each other. It is hard to say physically what kind of microstructure two or more overlapped ITZ regions would have, but in this model, ITZ regions can smoothly overlap. This definition then clearly divides the cement paste matrix into disjoint parts – the region within the ITZ thickness of an aggregate surface, called the ITZ paste, and all the other paste, called the bulk paste, so that $\phi_p = \phi_B + \phi_{ITZ}$, where ϕ_p is the total paste volume fraction, ϕ_B is the part of the paste in the bulk regions, and ϕ_{ITZ} is the part of the paste within the ITZ region.

These volume fraction parameters can be computed from the aggregate size distribution if we also assume that the aggregates are spherical, and that the volume of ITZ overlaps is small compared to the volume of the total ITZ regions. One way is to take a certain mass of aggregate that follows a given size distribution, and take the difference of the volume with and the volume without the ITZ regions. This gives the total volume occupied by the ITZ regions. In the past, the work by Lu and Torquato [52] has been used to determine the total ITZ volume including overlaps, but subsequent work has shown that for a typical concrete, this overlap volume is usually small compared to the total ITZ volume [31]. In this paper, the “surface area” approach has been used, where the ITZ volume is determined by multiplying the surface area of the aggregates with the uniform thickness of the ITZ layer, which is assumed to be 14 μm . For all the systems considered, using the more exact Lu–Torquato formula [31,52] would have changed the ITZ volume fractions by at most 10% of their values.

Although geometrical ideas are clearly emphasized in the hard-core soft-shell model, one must nevertheless also consider effects of material properties such as elastic moduli. In the literature, one finds a certain value property assigned to the bulk paste, usually the property of the cement paste component of the concrete measured separately, and then a value for the ITZ regions is guessed. A more careful choice of these parameters for ionic diffusivity has been demonstrated using multi-scale microstructural modeling [30,32]. The next section explains how the ITZ and bulk paste elastic properties can be more carefully chosen, in a similar way.

4.2. Numerical simulation of the microstructure

The VCCTL cement hydration module, which is an extension of the microstructural development model CEMHYD3D [53,54] places cement particles randomly in a box, dissolves, diffuse, and reacts the particles to form a cement paste microstructure. It has had the long capability to place particles against a slab surface to create an ITZ [6,55]. Fig. 2 shows the geometry that is typically used, with periodic boundary conditions. Since cement particles are usually at least an order of magnitude smaller than aggregate

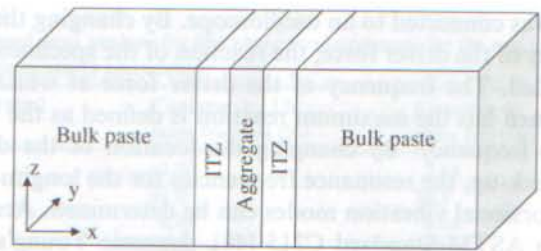


Fig. 2. Shape and construction of box for simulating geometry and elastic properties of ITZ and bulk cement paste.

particles, locally the aggregate surface looks similar to a flat slab, so this geometry is usually adequate for simulating the ITZ regions around a single aggregate particle. With the 10 voxel thick aggregate slab in the middle of the box, an ITZ is formed on both sides of the slab. Results for each system are then averaged over both sides of the slab. System sizes used ranged from 74 to 194 voxels in the x -direction, normal to the slab, while the y and z dimensions of the box were usually 100×100 voxels. For the smallest x -value used, 74, the dimensions of the y and z directions were taken to be 150 voxels, to allow more room for the larger particles in the particle size distribution. The physical size of each voxel was taken to be $1 \mu\text{m}^3$, which is the typical size used for this model [56].

Fig. 3 shows the w/c ratio for each 1 μm -thick slice parallel to the aggregate surface. The simulation used real-shape cement particles, which is an extension of the CEMHYD3D model [57,58]. This parameter is calculated by adding up all the cement volume in a given slice, and using the water volume in that slice to calculate the w/c ratio for that slice. The results in Fig. 3 have been averaged over three independent systems. One could plot the results in terms of porosity, but we choose to use w/c ratio, as that is a common parameter used in concrete mix designs. Note the large increase in w/c ratio as the aggregate surface is

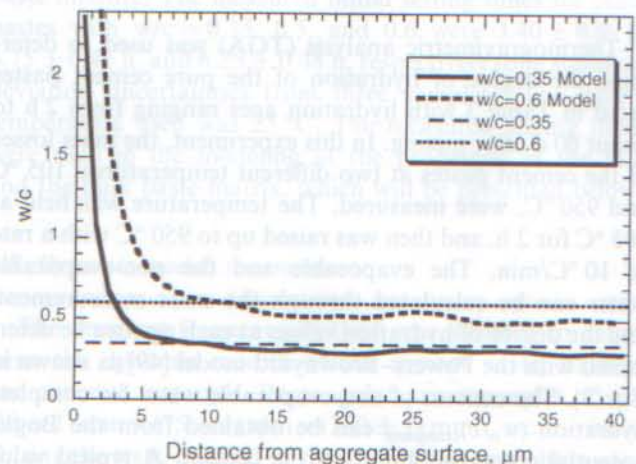


Fig. 3. Model results for w/c vs. distance from aggregate surface (μm) for average $w/c = 0.35$ (system 9m) and $w/c = 0.6$ (system 14m). Both systems had the same value of $V_{ITZ}/V_{paste} = 0.346$.

approached. The horizontal lines indicate the average w/c value for the system. One can clearly see that in the bulk regions, the w/c ratio per slice is less than the nominal, average value, to make up for the ITZ regions, where the w/c ratio is larger than the average value. The average w/c ratio for each system is equal to the nominal w/c ratio, 0.35 or 0.6. For these systems, the limit of the ITZ would be taken at 14 μm . The size of the box in Fig. 2 in the x -direction, which is the direction normal to the aggregate slab face, is chosen so that the ratio of the volume of the ITZ region to that of the bulk paste region is the same as in one of the real mortars or concretes studied in this paper [30].

Fig. 4 shows four slices from a system like that shown in Fig. 2, at four different degrees of hydration. The system was sliced perpendicular to the slab aggregate, so the thickness of the aggregate is seen in each slice. By eye, it is quite hard to see the higher porosity in the two ITZ regions, since it is only 14 pixels thick in these images. In the model, CH precipitation on aggregate surfaces was not allowed, as this gave the best agreement with experimental results for the CH profile within the ITZ [2,3].

Before hydration, Fig. 3 showed that the w/c ratio could be computed as a function of distance from the aggregate interface. For our simplified three-phase model, we want to treat the ITZ as a uniform region and the bulk paste

as a uniform region as well. We can therefore average over the 14 μm thick ITZ region and separately average over the bulk region to get an average value of w/c in each region. We have done so, again averaged over three independent microstructures (uncertainties are one standard deviation over the three microstructures). One finds the total cement in each region to find the average value of w/c ratio for each region. One cannot simply average over the slice-to-slice w/c ratio. The results are listed in Table 5, for all the systems containing aggregates. The system size in the x -direction, normal to the aggregate slab, has been adjusted in each case so as to closely match the experimental ratio of $\text{Vol}_{\text{ITZ}}/\text{Vol}_{\text{paste}}$ as given in Table 5, where $\text{Vol}_{\text{paste}}$ is the sum of ITZ and bulk paste divided by the total composite volume and equals $1 - \text{Vol}_{\text{agg}}$, where Vol_{agg} is the volume fraction of aggregate (see Table 3). For example, for the 11m system, the ratio of $\text{Vol}_{\text{ITZ}}/\text{Vol}_{\text{bulk}} = 8.4/46.8 = 0.179$. The dimensions of the system had 14 voxels for the ITZ and 78 voxels for the bulk paste, or a ratio of $14/78 = 0.179$. The total system size in the x -direction, 174, is made up of 82 voxels of paste on both sides of the 10 voxel thick aggregate slab. It can be seen in Table 5, for each nominal w/c ratio, that the average w/c ratio in the ITZ region was roughly independent of aggregate volume, depending mainly on the overall average w/c ratio of the total paste matrix.

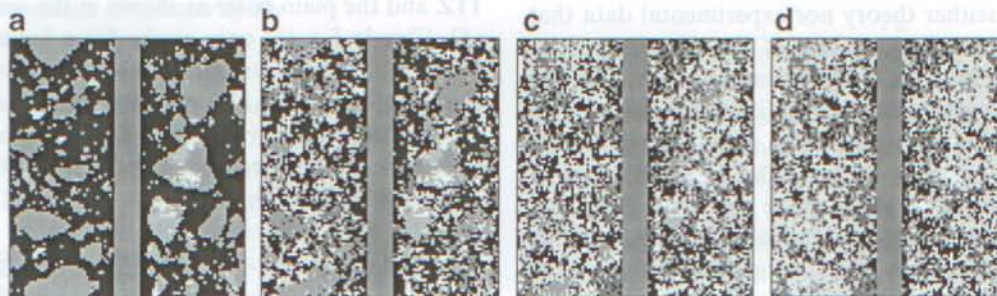


Fig. 4. Slices of the microstructure of system 5m at different degrees of hydration: (a) $\alpha = 0.0$, (b) $\alpha = 0.352$, (c) $\alpha = 0.644$, and (d) $\alpha = 0.805$.

Table 5
Simulated w/c ratio in ITZ and bulk paste matrix

No.	w/c (global)	(w/c) _{ITZ}	(w/c) _{bulk}	Vol _{ITZ} (%)	Vol _{paste} (%)	Vol _{agg} (%)
2m	0.5	0.738 ± 0.04	0.464 ± 0.005	8.9	52.4	47.6
3c	0.5	0.749 ± 0.023	0.458 ± 0.003	6.6	35.2	64.8
4c	0.5	0.695 ± 0.014	0.464 ± 0.002	6.2	32.5	67.5
5m	0.5	0.711 ± 0.02	0.427 ± 0.006	12.2	35.2	64.8
Avg	0.5	0.723 ± 0.025				
7m	0.35	0.476 ± 0.025	0.323 ± 0.004	9.9	47.3	52.7
8m	0.35	0.464 ± 0.005	0.317 ± 0.001	10.9	41.8	58.2
9m	0.35	0.451 ± 0.011	0.307 ± 0.004	12.2	35.3	64.7
Avg	0.35	0.464 ± 0.013				
11m	0.6	0.928 ± 0.05	0.564 ± 0.005	8.4	55.2	44.8
12c	0.6	0.934 ± 0.044	0.559 ± 0.004	6.3	37.9	62.1
13m	0.6	0.768 ± 0.009	0.503 ± 0.005	13.2	29.5	70.5
14m	0.6	0.850 ± 0.042	0.515 ± 0.011	12.2	35.2	64.8
Avg	0.6	0.870 ± 0.078				

4.3. Modeling the elastic properties of ITZ

Due to the complex structure of the ITZ region and the constraints of existing measuring techniques [59,60], it is difficult to determine the local mechanical properties in the ITZ. Before resorting to direct simulation of the ITZ microstructure and elastic properties, we try a hybrid experimental-simulation approach, making use of the w/c ratios determined by simulation along with the experimentally measured cement paste elastic moduli to determine the ratio of ITZ and bulk cement paste to plain paste values. This approach is gradually built up from the simplest assumptions to more sophisticated, and hopefully more accurate, assumptions.

It is often assumed that the moduli in the ITZ are less than those in the bulk paste by a fixed ratio. In other words, the Young's modulus of ITZ can be presented by the following expression:

$$E_{ITZ} = aE_{pp} \tag{4}$$

where *a* is a constant with a proposed value between 0.2 and 0.8 [8,13–15,39,57], and *E_{pp}* is the Young's modulus of the corresponding plain paste, which can be easily measured. Along with this assumption, one also usually assumes that outside the ITZ regions, the bulk paste elastic moduli are the same as the plain paste moduli.

Although Eq. (4) gives relatively good simulation results for the elastic properties of concrete composites (as will be shown), there is neither theory nor experimental data that can support these assumed values of the parameter *a* or assuming that the bulk paste elastic moduli values are the same as the plain paste values. In addition, no change with hydration age is usually considered in the formula. As discussed in the previous section, the ITZ w/c ratio is higher than the overall average value specified in the mix design. Taking sample 2m listed in Table 3 as an example, the ITZ w/c ratio becomes 0.738, compared to the overall average value of 0.5. Due to this reason, the parameter *a* in Eq. (4) should be considered to be a function of hydration age, since the elastic properties of cement pastes with various w/c ratios develop at different rates under the same curing conditions [61].

The following model for the elastic properties of the ITZ, compared to those of plain paste, is proposed. Taking plain paste as a reference, the ratio of the dynamic Young's moduli of ITZ and the corresponding plain paste is assumed to be a function of hydration age as shown in Eq. (5) and illustrated schematically in Fig. 5.

$$R_1 = R_{1u} \frac{k(t - t_0)^{\alpha}}{1 + k(t - t_0)^{\alpha}} \tag{5}$$

In the equation, *k* and *α* are two parameters whose value can be determined by regression. *t* is the hydration age. *t₀* is the initial setting time of the plain paste, which can be determined by the Vicat needle test. It is assumed that no elastic moduli can be obtained before the initial setting time. Thus, *R₁* = 0 when *t* < *t₀*, since the ITZ region sets la-

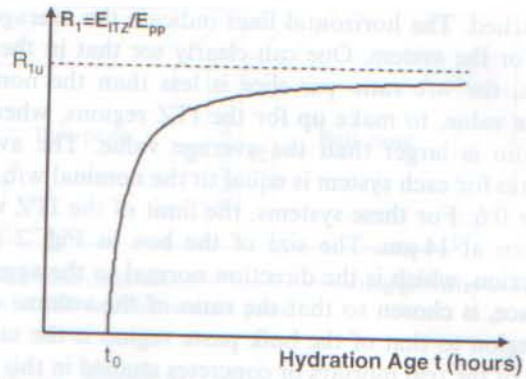


Fig. 5. Modeling the ITZ elastic properties.

ter than the plain paste due to the increase in the w/c ratio. The effect of w/c ratio on setting time has been seen before [62,63] and also in this present work.

The parameter *R_{1u}* can be determined experimentally. In this research, the dynamic moduli of plain paste with w/c ratios ranging from 0.35 to 0.6 were measured up to 28 d after casting. A hyperbolic function was used to describe the development of degree of hydration and the dynamic Young's modulus [64–66]. The ultimate Young's modulus, *E_u*, of each paste was obtained from the regression. *E_u* can be regarded as a power-law function of w/c ratio as shown in Fig. 6 and described in Eq. (6). Thus, the parameter *R_{1u}* can be obtained by considering the ratio of the w/c ratios of ITZ and the plain paste as shown in the second part of Eq. (6). Clearly Eq. (6) only works for a limited range of w/c ratio, as *E_u* goes to infinity as the w/c ratio goes to 0. One could also use the porosity instead of the w/c ratio as the independent variable in Eq. (6). This choice of variable may be of more use in blended cements, where the w/c ratio is a less useful parameter.

$$E_u = 7.9(w/c)^{-1.08}; \quad R_{1u} = \frac{E_{u-ITZ}}{E_{u-pp}} = \left(\frac{(w/c)_{ITZ}}{(w/c)_{pp}} \right)^{-1.08} \tag{6}$$

Similarly, the dynamic Young's moduli of a cement paste at a certain hydration age can be regarded as a function of the w/c ratio using an expression similar to Eq. (6). However, a different value of the coefficient and index should be used according to the hydration age of the

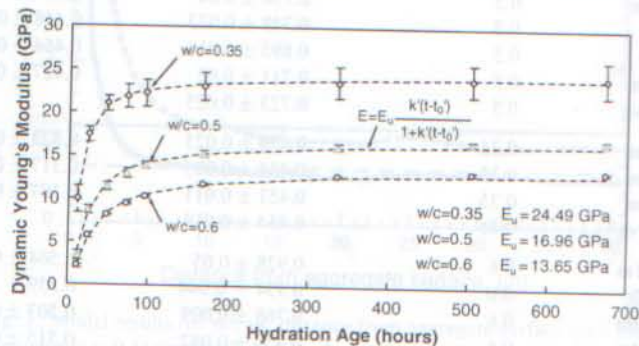


Fig. 6. Determination of the parameter *R_{1u}*.

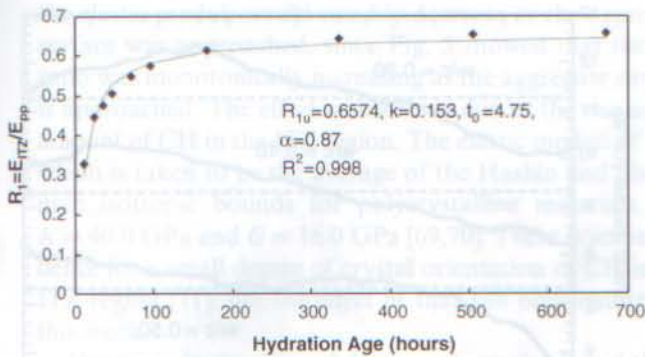


Fig. 7. R_1 values of mortar 2m.

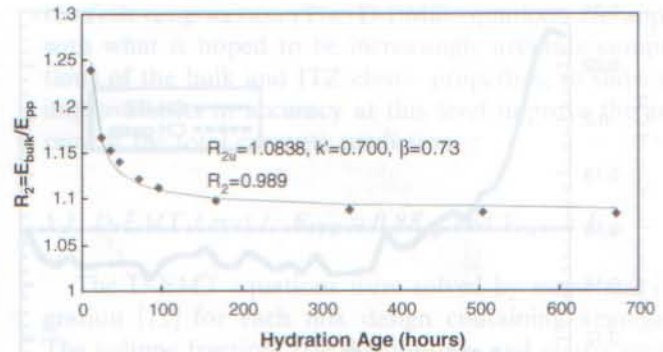


Fig. 9. R_2 values of mortar 2m.

cement paste. R_1 values can be obtained directly by inserting the ITZ w/c ratio and the plain pastes at various hydration ages using the measured data displayed in Fig. 6. The one standard deviation error bars, calculated over three samples, in Fig. 6 that are shown for the w/c = 0.35 data are typical of the experimental uncertainties for all the elastic measurements, in this and subsequent figures (error bars not shown), measured over four nominally identical samples. The R_1 values of mortar 2m are given in Fig. 7 as an example of this process. Thus, the ITZ elastic properties of our cement-based composites can be modeled in this way.

4.4. Modeling the elastic properties of the bulk paste matrix

Just like for the ITZ phase, the corresponding change in the properties of the bulk paste matrix should be considered. Again, the elastic property of the plain paste is used as a reference. The ratio of the elastic properties between the bulk paste matrix and the plain paste, R_2 , is again assumed to be a function of the hydration age. The development curve of R_2 can be described by Eq. (7) and is shown in Fig. 8.

$$R_2 = R_{2u} + \frac{k'}{(t - t_0)^\beta}; \quad R_{2u} = \left(\frac{(w/c)_{bulk}}{(w/c)_{pp}} \right)^{-1.08} \quad (7)$$

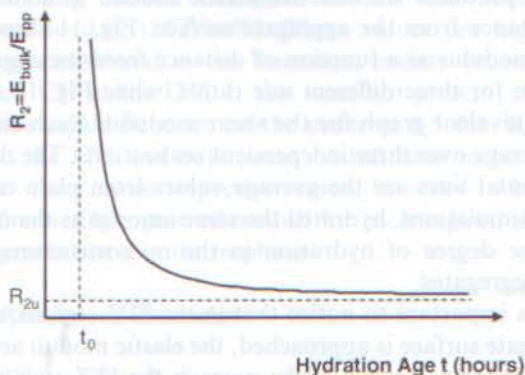


Fig. 8. Modeling the elastic moduli of the bulk paste matrix.

R_{2u} can be obtained from Eq. (7), where the w/c ratios of the bulk paste matrix and the corresponding plain paste are considered. t and t_0 are defined in Eq. (6). k' and β are parameters that can be obtained via regression. When $t < t_0$, R_2 diverges, since the bulk paste matrix sets earlier than the plain paste due to the decrease in the w/c ratio in the bulk matrix. The form of Eq. (7) was chosen in analogy with Eq. (6), and to obtain the proper asymptotic behavior at $t = t_0$ and $t = \infty$.

Similar to the R_1 values, the R_2 values of mortar 2m are given in Fig. 9 as an example of this process. Thus, the bulk paste elastic properties of our cement-based composites can be modeled in this way as a function of age.

4.5. Further modification of R_1 and R_2

Previously, in this paper and in other papers [25,26], it has been assumed that the elastic moduli in the ITZ zone varied with w/c ratio just as plain cement paste varied with w/c ratio. Although there is a gradient in w/c ratio in the ITZ, if there were no redistribution of hydration products, then this assumption would be true. However, it is known from SEM studies that there is, for example, a gradient of CH in the ITZ where the amount of CH is higher the nearer the aggregate surface is approached [2,3]. The relative amounts of hydration products are then different from those of plain cement paste in the ITZ. Our hybrid experimental-simulation approach breaks down at this point, since we do not have experimental data on this kind of modified ITZ paste, but our VCCTL microstructure model, in combination with the finite element method, can simulate this effect [61] and so can be used to correct the hybrid approach. Ref. [61] showed how accurate this simulation approach can be for cement paste, $\pm 5\%$, so the simulation results in the ITZ region will be accurate as well. Fig. 2 showed the basic structure of the computational system. Once the initial cement is hydrated, analysis can be done of the hydrated phases.

A system similar to but different from all the systems listed in Table 3 was chosen to explore the actual elastic moduli in the ITZ region could be affected by the CH content. Fig. 10 shows the CH volume fraction as a function of

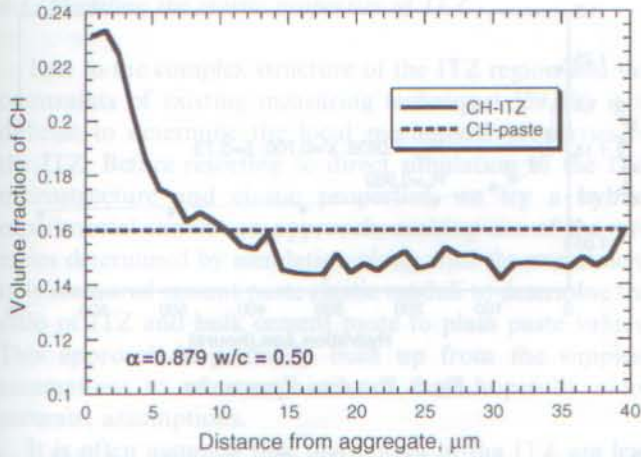


Fig. 10. Showing the CH volume fraction in an 0.5 w/c ratio composite as a function of distance from the aggregate surface.

distance from the (flat) aggregate surface for a w/c = 0.50 paste with a degree of hydration of 0.879 as computed by the VCCTL hydration model. The system used for Figs. 10–13 was 100 voxels in each direction, with an aggregate slab thickness of 20 voxels. This meant that the ratio of ITZ volume to bulk paste volume was $14/40 = 0.35$, almost identical to the 5m, 9m, and 13m systems. The higher amount of CH in the ITZ region is offset by a lower amount in the bulk paste region [2,3]. The dashed line is the average value from plain paste simulations – there would actually be some finite size noise in this horizontal line if the unaveraged values were used. The areas under the two curves are identical, since both systems had an average w/c ratio of 0.5.

Methods have been developed for computing the linear elastic moduli of an arbitrary shape and size 3D image [67,68] and applied to cement paste microstructures [61]. These methods have been incorporated into the VCCTL

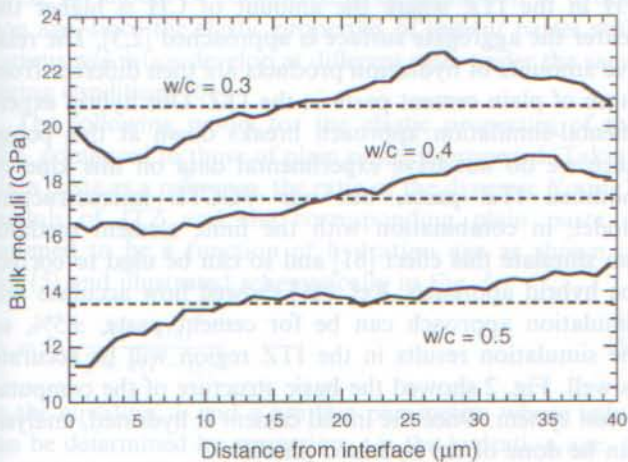


Fig. 11. Simulated bulk modulus as a function of distance from the aggregate surface, for three different w/c ratio pastes using the same cement (averaged over three realizations). The dashed lines are the plain paste results for that w/c ratio.

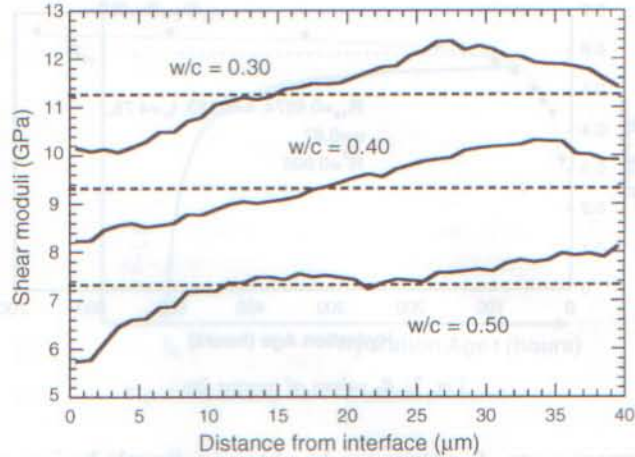


Fig. 12. Simulated shear modulus as a function of distance from the aggregate surface, for three different w/c ratio pastes using the same cement (averaged over three realizations). The dashed lines are the plain paste results for that w/c ratio.

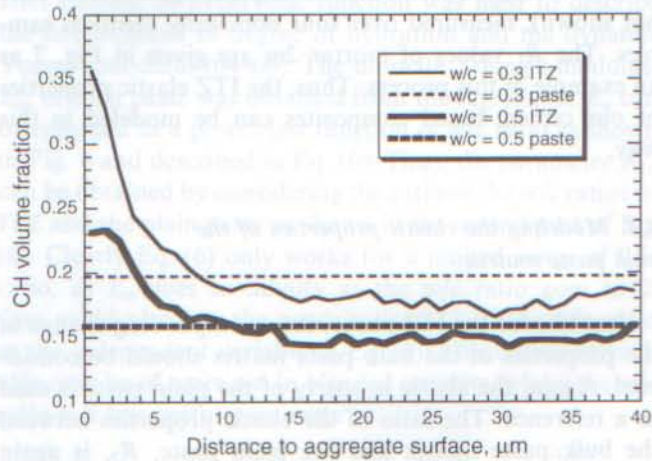


Fig. 13. The CH profiles, as a function of distance from the aggregate surface, for the w/c = 0.3 and 0.5 systems shown in Figs. 11 and 12.

software. Since they give the average stress and strain, as tensors, in each voxel, each one-voxel-thick slab that is parallel to the aggregate surface can be averaged over, which produces the effective elastic moduli as a function of distance from the aggregate surface. Fig. 11 shows the bulk modulus as a function of distance from the aggregate surface for three different w/c ratios, while Fig. 12 shows the equivalent graph for the shear modulus. Each curve is an average over three independent realizations. The dashed horizontal lines are the average values from plain cement paste simulations, hydrated the same amount as the overall average degree of hydration in the microstructures with slab aggregates.

It is important to notice that in the ITZ regions, as the aggregate surface is approached, the elastic moduli actually increase for w/c = 0.3. If the paste in the ITZ region were equivalent to plain paste with the same w/c ratio, then

the elastic moduli would steadily decrease as the aggregate surface was approached, since Fig. 3 showed that the w/c ratio was monotonically increasing as the aggregate surface is approached. The effect seen here is due to the rise in the amount of CH in the ITZ region. The elastic moduli of CH, which is taken to be the average of the Hashin and Shtrikman isotropic bounds for polycrystalline materials, are $K = 40.0$ GPa and $G = 16.0$ GPa [69,70]. There is some evidence for a small degree of crystal orientation of CH in the ITZ region [71], but the effect of that has been ignored in this work.

However, in the w/c = 0.5 curves, both the K and the G curves do not increase as the aggregate surface is approached, but continue to decline. The w/c = 0.4 curves tend to flatten out as the aggregate surface is approached. Fig. 13 sheds light on this varied behavior. In Fig. 13, the CH profiles for w/c = 0.3 and w/c = 0.5 curves are displayed. Notice that the gradient in CH is significantly larger for the w/c = 0.3 system than for the w/c = 0.5 system. The horizontal lines are the pure paste results. Apparently, at the higher w/c ratios, the overall decrease in cement and increase in porosity as the aggregate surface is approached overcomes the increasing amount of CH in this same region, so that the elastic moduli decrease or at best flatten out. From these results, it would seem that the critical value of w/c ratio is about 0.4, at least for the cement used in this study, where the increased CH can start to overcome the effect of the increased porosity on the elastic moduli in the ITZ region.

All the cement composite systems listed in Table 3 were simulated by controlling the ratio of ITZ paste to bulk paste and the overall w/c ratio. The elastic moduli were averaged over three independent configurations and also averaged over the ITZ and bulk paste regions to give refined values of R_1 and R_2 . A closer examination of some results is instructive. The 9m and 14m systems had the same volume fraction and size distribution of aggregates, with different w/c ratios (0.35 for 9m and 0.6 for 14 m). For system 9m, the highest model degree of hydration considered was 0.788. At this point, the ratios of Young's moduli and shear moduli were roughly equal to 0.88 (ITZ/bulk). For system 14m, the highest model degree of hydration considered was 0.81. At this point, the ratios of Young's moduli and shear moduli were both roughly equal to 0.82 (ITZ/bulk). These values are higher than those considered in the literature, mainly because of the extra CH in the ITZ. If this were not present, then these ratios would be more on the order of 0.5–0.6. Remember that the ITZ and bulk paste moduli have to be averaged over their entire respective region, in order to be able to define a single pair of moduli for each region, since each region is not a uniform phase.

5. Results and discussion

The computed elastic properties of concrete and mortar composites using D-EMT are presented and discussed in

the following section. The D-EMT equations are applied with what is hoped to be increasingly accurate computations of the bulk and ITZ elastic properties, to show that improvements in accuracy at this level improve the accuracy of the total concrete prediction.

5.1. D-EMT Level 1: $E_{ITZ} = 0.8E_{pp}$ and $E_{bulk} = E_{pp}$

The D-EMT equations were solved by numerical integration [72] for each mix design containing aggregates. The volume fraction, size distribution, and elastic properties of aggregates, ITZ thickness, and the elastic properties of ITZ and bulk paste matrix were used as inputs in the simulation. In order to first demonstrate that D-EMT had even a hope of computing the elastic properties of a concrete composite, the assumption that $E_{ITZ} = 0.8E_{pp}$ and $E_{bulk} = E_{pp}$ was used. The comparison of the dynamic shear moduli between the experimental data and the simulation results is plotted in Fig. 14 for composite 3c. We note that the theory presented in the previous section works just as well for the shear modulus as for the Young's modulus. For the sake of reference, the Level 0 curve is shown in Fig. 14, where Level 0 means that the width of the ITZ has been set to zero and the matrix has been made equal to plain cement paste of the given w/c ratio. This causes the D-EMT to become the same as usual D-EMT [28,29]. The Level 0 curve falls significantly above the experimental data, indicating that the neglect of the ITZ regions overestimates the elastic effect of the aggregate inclusions, and does not give the correct curve shape.

The computed D-EMT results for the dynamic Young's moduli of this composite are very similar to that of the dynamic shear moduli, and are not plotted in the figure. From Fig. 14, it can be noted that the shape of the D-EMT curve is very similar to the development trend of the dynamic shear moduli that are obtained experimentally with the resonant frequency method. This result indicates that the D-EMT has the potential to be used for computing the elastic properties of concrete composites, even when the volume fractions of the aggregates are well beyond the dilute limit. A detailed comparison

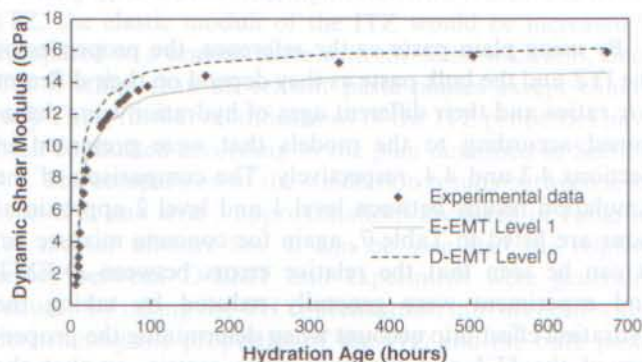


Fig. 14. Concrete 3c (D-EMT Level 1).

Table 6
Comparison of D-EMT and experimental data for concrete mixture 3c (Level 1 $E_{ITZ} = 0.8E_{pp}$; $E_{bulk} = E_{pp}$)

Hydration age, h	E_{exp} (GPa)	E_{D-EMT} (GPa)	Δ_E (%)	G_{exp} (GPa)	G_{D-EMT} (GPa)	Δ_G (%)
7	3.67	3.99	23.8	1.34	1.66	8.6
10	8.19	10.2	28.8	3.02	3.89	24.8
14	15.6	18.8	18.7	6.29	7.47	20.9
18	20.7	21.8	12.1	7.84	8.79	5.4
24	24.3	24.5	4.9	9.46	9.92	0.9
48	30.2	28.5	-3.6	12.1	11.6	-5.5
72	32.8	30.4	-5.2	13.2	12.5	-7.1
96	34.2	31.6	-5.2	13.8	13.1	-7.4
168	36.0	33.1	-5.2	14.4	13.7	-7.9
336	37.5	34.1	-5.9	15.2	14.3	-9.0
504	38.3	34.7	-7.6	15.6	14.4	-9.3
672	39.2	35.0	-8.1	15.9	14.6	-10.7

between experimental and D-EMT results is listed in Table 6, where

$$\Delta_E(\%) = \frac{E_{D-EMT} - E_{exp}}{E_{exp}} \times 100\%;$$

$$\Delta_G(\%) = \frac{G_{D-EMT} - G_{exp}}{G_{exp}} \times 100\% \quad (8)$$

In Table 6, it can be noted that at early age (less than 24 h), the D-EMT results are larger than those of the experimental data, by as much as 30%. However, with increasing hydration age, the D-EMT results become smaller than the experimental results, with the relative errors approaching -10%. The comparisons of the D-EMT and the experimental results for other mortars or concretes considered were similar. This indicates that a constant ratio between the properties of ITZ and the corresponding plain paste for all hydration ages is unreasonable. If the condition $E_{ITZ} = 0.5E_{pp}$ was used in the D-EMT calculation as other researchers did [8,14,16,41,60], the errors would be even larger than the current values. The contrast of the elastic properties between ITZ and the plain paste ($R_1 = E_{ITZ}/E_{pp}$) should be considered to be a function of the hydration age, since the elastic properties of the ITZ and the bulk paste matrix both change with hydration in different ways.

5.2. D-EMT Level 2: $E_{ITZ} = R_1E_{pp}$; $E_{bulk} = R_2E_{pp}$

By using plain paste as the reference, the properties of the ITZ and the bulk paste as they depend on their different w/c ratios and their different ages of hydration were determined according to the models that were presented in Sections 4.3 and 4.4, respectively. The comparison of the simulation results between level 1 and level 2 approximations are listed in Table 7, again for concrete mixture 3c. It can be seen that the relative errors between D-EMT and experiment were generally reduced by taking the hydration effect into account when determining the properties of the ITZ and the bulk paste matrix, so that the D-EMT curve moved closer to the experimental data.

Table 7
Comparison of D-EMT results for Level 1 and Level 2 assumptions for concrete mixture 3c (Level 1: $E_{ITZ} = 0.8E_{pp}$; $E_{bulk} = E_{pp}$; Level 2: $E_{ITZ} = R_1E_{pp}$; $E_{bulk} = R_2E_{pp}$)

Hydration age, h	D-EMT Level 1		D-EMT Level 2	
	Δ_E (%)	Δ_G (%)	Δ_E (%)	Δ_G (%)
7	8.6	23.8	-22.2	-10.5
10	24.8	28.8	9.7	10.9
14	20.9	18.7	13.9	11.6
18	5.4	12.1	1.8	8.1
24	0.9	4.9	-0.8	3.2
48	-5.5	-3.6	-5.1	-3.2
72	-7.1	-5.2	-6.2	-4.2
96	-7.4	-5.2	-6.3	-4.0
168	-7.9	-5.2	-6.5	-3.8
336	-9.0	-5.9	-7.6	-4.4
504	-9.3	-7.6	-7.8	-6.0
672	-10.7	-8.1	-9.2	-6.6

Another two examples of the comparisons between the D-EMT results with level 1 and level 2 assumptions are plotted in Fig. 15 for mortars 8m and 13m. Since the results for the dynamic Young's moduli were very similar to those of the dynamic shear moduli, only the results for dynamic shear moduli are plotted. It can be seen that for both mortars, the relative errors between D-EMT and experiment are always improved by applying the models of ITZ and the bulk paste matrix properties as proposed in this section.

Since Fig. 15 showed that the Level 2 D-EMT approximation did quite a good job of matching the experimental

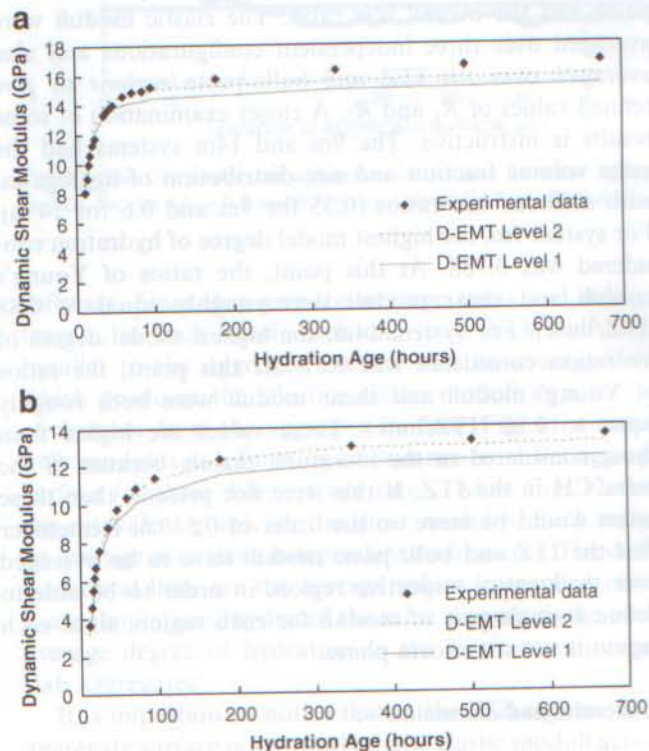


Fig. 15. Comparison of D-EMT with experiment with level 1 and level 2 assumptions for mixtures (a) 8m and (b) 13m.

Table 8

Comparison of the D-EMT results between mortars having different aggregate volume fractions but the same average w/c ratio paste

Hydration age (h)	7m		8m		9m	
	Δ_E (%)	Δ_G (%)	Δ_E (%)	Δ_G (%)	Δ_E (%)	Δ_G (%)
12	1.8	3.5	5.2	10.0	12.4	16.8
24	5.3	3.6	7.5	8.0	12.0	12.1
48	-1.2	-1.8	1.4	2.5	5.6	7.5
72	-3.3	-4.5	-1.5	-0.8	1.9	4.1
96	-4.5	-4.5	-3.1	-0.9	0.2	3.2
168	-5.5	-6.5	-3.6	-3.0	-0.8	2.9
336	-7.0	-7.3	-5.4	-4.2	-2.3	-0.9
504	-7.6	-8.0	-6.4	-5.1	-2.8	-2.0
672	-7.7	-8.8	-6.6	-5.5	-3.2	-2.7

results, we use the Level 2 D-EMT to investigate some choices of systems. To help sort out the dependence of the D-EMT results on different microstructural parameters, mortars with the same paste matrix, but various volume fractions of aggregates, were compared. The D-EMT results for mortars 7m, 8m and 9m are shown in Table 8 using the Level 2 assumptions for R_1 and R_2 . The overall paste matrix for these mortars is the same since they had the same w/c ratio = 0.35. However, the volume fraction of aggregates changes from 53% to 58% to 64% (7m → 8m → 9m). In Table 8, it can be noted that, for later ages, the relative errors of the D-EMT results decrease as the aggregate volume fraction increases. For example, at 28 d (672 h), the relative error between D-EMT and experiment for the dynamic shear modulus decreases from -8.8% (7m) to -6.6% (8m) to -2.7% (9m). The reason for this behavior is likely to be the contrast between the elastic properties of the bulk paste matrix and the effective aggregate. For these three mortars, the elastic properties of the ITZ are similar, because the overall average w/c ratios used in the mix design were the same. However, due to the high aggregate volume fraction in mortar 9m, mortar 9m has the highest volume fraction of ITZ in these three mortars, which results in the lowest value of the bulk paste w/c ratio. This implies that the bulk paste matrix in mortar 9m is stiffer than that in mortar 8m and 7m and closer to the aggregate value. Therefore, the elastic moduli contrast between the effective aggregate and the bulk paste matrix is smallest for this mortar out of the three mortars. It is known that D-EMT works better as the elastic contrast between inclusion and matrix becomes closer to unity [28,29].

Next, concrete and mortar composites with the same volume fraction of aggregates but different aggregate size distributions were compared. The relative errors between the D-EMT simulations and the experimental data are listed in Table 9. Comparing the results shown in the table for concrete 3c and mortar 5m, it can be noted that the relative errors for mortar 5m are smaller than those for concrete 3c. Both 3c and 5m had the same w/c ratio, 0.5, but different aggregate size distributions. In mortar 5m, there is a higher volume fraction of ITZ than in concrete 3c since

Table 9

Comparison of D-EMT with experiment for composites with the same aggregate volume fraction but different paste matrices

Hydration age (h)	3c		5m		9m		14m	
	Δ_E (%)	Δ_G (%)						
12	9.7	8.4	1.9	-5.1	12.4	16.8	-16.4	-12.5
24	-0.8	3.2	-0.6	2.1	12.0	12.1	-12.6	-7.3
48	-5.1	-3.2	-2.0	0.02	5.6	7.5	-9.1	-4.8
72	-6.2	-4.2	-3.2	-0.6	1.9	4.1	-9.7	-6.8
96	-6.3	-4.1	-3.0	-1.0	0.2	3.2	-9.6	-7.9
168	-6.5	-3.8	-3.2	-1.5	-0.8	2.9	-9.2	-7.4
336	-7.6	-4.4	-4.3	-1.0	-2.3	-0.9	-9.3	-6.7
504	-7.8	-6.0	-4.3	-1.7	-2.8	-2.0	-9.9	-9.0
672	-9.2	-6.6	-4.4	-1.7	-3.2	-2.7	-9.1	-9.3

the aggregates used in mortar 5m have a smaller average diameter than those used in the concrete 3c and therefore a larger surface area. This decreases the w/c ratio in the bulk paste matrix of mortar 5m and thus increases the bulk paste elastic moduli. The contrast of the elastic properties between the effective aggregate and the bulk paste matrix for mortar 5m is smaller than that of 3c, which is responsible for the higher accuracy of D-EMT for this case.

Similarly, we consider three systems that had the same volume fraction and size distribution of aggregates but with different paste matrices. Looking at Table 9, it can be seen that the relative errors for mortar 14m (w/c = 0.6) are larger than those for 5m (w/c = 0.5) and 9m (w/c = 0.35). Again, this is due to the contrast of the elastic properties of the effective aggregate and the bulk paste matrix. Mortar 14m has a much higher w/c ratio than mortars 5m or 9m and so has the least stiff bulk paste matrix (see Table 5), which causes a larger elastic moduli contrast between the effective aggregate and the bulk paste matrix. This higher contrast degrades somewhat the accuracy of the D-EMT approximation.

5.3. D-EMT Level 3: $E_{ITZ} = R_1/E_{pp}$

The accuracy of the D-EMT computation can be further improved by considering the redistribution of hydration products that occur in the ITZ and bulk paste regions, particularly CH. Due to the high concentration of CH in the ITZ, the elastic moduli of the ITZ would be increased if compared to a cement paste with the same w/c ratio, since CH is stiffer than all cement paste phases except clinker [61]. Thus, further modifications of the ITZ properties have been conducted according to the plan described in Section 4.5. The comparison of the simulation results between level 1, level 2, and level 3 approximations are listed in Table 10 for mortar mixture 8m. It can be seen that the relative errors between D-EMT and experiment were generally reduced by taking the CH concentration into account when determining the properties of the ITZ and the bulk paste matrix. Using this modified elastic contrast between ITZ and bulk paste, new D-EMT results for mortars and

Table 10
Comparison of Level 1, 2, and 3 D-EMT results for system 8m (Level 1: $E_{ITZ} = 0.8E_{pp}$; $E_{bulk} = E_{pp}$; Level 2: $E_{ITZ} = R_1E_{pp}$; $E_{bulk} = R_2E_{pp}$ Level 3: $E_{ITZ} = R_1/E_{pp}$)

Hydration age (h)	D-EMT Level 1		D-EMT Level 2		D-EMT Level 3	
	ΔE (%)	ΔG (%)	ΔE (%)	ΔG (%)	ΔE (%)	ΔG (%)
12	1.3	5.9	5.2	10.0	2.8	7.5
24	3.6	4.1	7.5	8.0	7.8	8.3
48	-2.6	-1.5	1.4	2.5	2.0	3.2
72	-5.4	-4.8	-1.5	-0.8	-0.8	-0.1
96	-6.9	-4.9	-3.1	-0.9	-2.1	0.0
168	-7.4	-7.1	-3.6	-3.0	-2.1	-1.8
336	-9.0	-8.0	-5.4	-4.2	-2.8	-1.7
504	-10.0	-8.7	-6.4	-5.1	-2.9	-1.6
672	-10.1	-9.1	-6.6	-5.5	-2.3	-1.2

concretes are plotted in Fig. 16 for some of the materials considered. In Fig. 16, it can be seen that for each composite, the D-EMT curve moves closer to the experimental data as the ratio of elastic moduli between ITZ and bulk paste is considered more and more accurately. However, the relative errors between D-EMT and experiment can be visually seen to be larger for the concrete with (c) $w/c = 0.6$ compared to the other two composites. Again, this is due to the larger aggregate-matrix elastic contrast for the composite having the least stiff matrix, since D-EMT works less accurately as the elastic contrast is increased.

6. Summary and conclusions

Real concrete has aggregates with random shape, a cement paste matrix with random microstructure, and ITZs that vary in microstructure from aggregate to aggregate. This paper has tried to address the ratio of elastic properties between ITZ and bulk paste, how to systematically and consistently treat the ITZ and bulk paste as uniform phases, and how to calculate mortar and concrete elastic moduli based on knowledge of the elastic moduli of individual constituents. Building on Nadeau's work [25,26], we believe we have made improvements in all three of these areas.

The modeling methodology of concrete elastic properties that was introduced in the paper was based on the combination of experiments and numerical simulation. Having precise experimental data on well-controlled systems that were made specifically for this study allowed a much better quantitative test of calculated elastic moduli. Numerical simulation of ITZ microstructure and properties allowed us to say something about properties in this region that would have been very difficult or impossible to obtain experimentally.

In the ITZ region, simulation results agreed with experiments showing that the porosity increases and so did the CH volume fraction as the aggregate surface was approached. The elastic contrast between bulk paste, which had an average w/c ratio smaller than the overall value, and the ITZ paste, which had an average w/c ratio larger than the overall value, was on the order of 0.7–0.9 at the least. These simulation results show that, except maybe at early age, the average stiffness of the ITZ paste compared to that of the bulk paste was lower than 1 but usually significantly larger than 0.5. The finite element method combined with the VCCTL hydration module do not capture the early age moduli very accurately [61]. These results do not address the respective fracture toughness of these regions, which do not have to linearly follow the elastic moduli trends. The width of the ITZ was taken to be equal to the median cement particle diameter size. Taking a different size would have changed these elastic ratios but not the overall results. Based on numerical simulations, this width was a rational, non-arbitrary choice for the ITZ width. Taking an arbitrary number based on fitting various

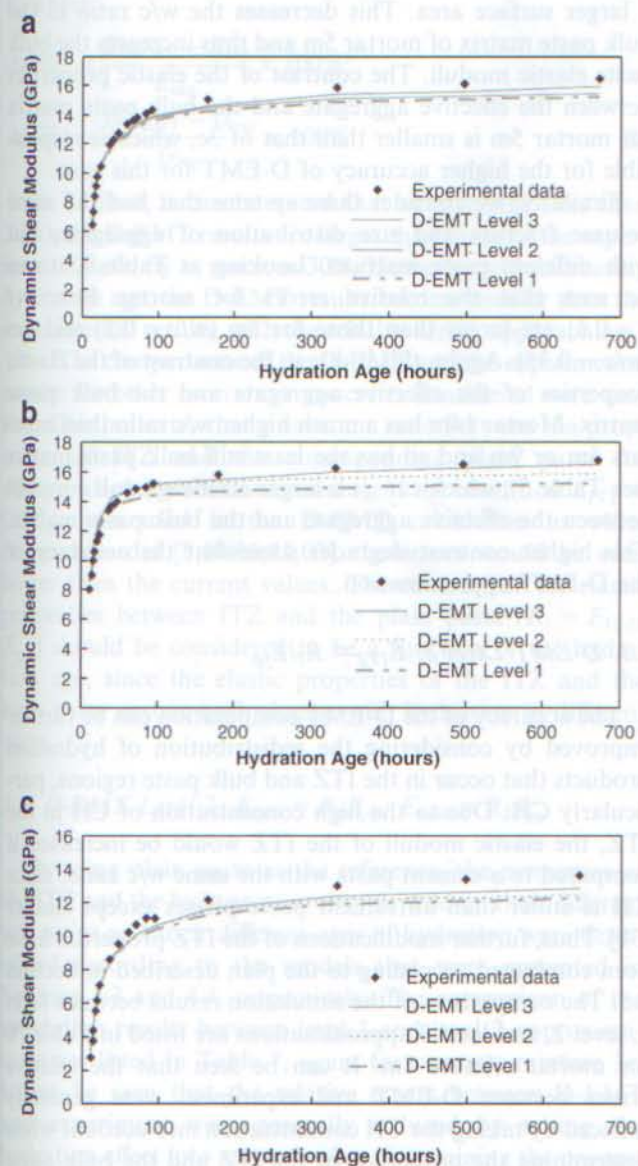


Fig. 16. Comparisons of D-EMT curves with experiment for (a) 4c ($w/c = 0.5$), (b) 8m ($w/c = 0.35$), and (c) 12c ($w/c = 0.6$).

kinds of effective medium theories to experimental results is not a reasonable approach.

Comparison with linear elastic (dynamic) experimental results have shown that concrete can be considered as a composite that consists of aggregate inclusions, ITZ regions, and the bulk paste matrix, where the properties of the ITZ and bulk paste regions were systematically determined using a fixed value for the ITZ width and averaging over the properties of each region to produce effective, uniform regions. It proved to accurately compute the elastic properties of concrete composites by using a differential effective medium theory (D-EMT).

At the first level of approximation, we assumed that the ratio of the elastic properties between the ITZ and the plain paste was an arbitrary constant. The computed elastic moduli then had a similar shape vs. age as compared to the resonant frequency experimental data. The accuracy of the D-EMT was systematically improved by considering the elastic moduli of the ITZ and the bulk paste matrix to be functions of hydration age, using a combination of experimental results for cement paste moduli and average ITZ and bulk paste w/c ratios computed from simulations and assuming that the cement paste in the ITZ and bulk paste regions were the same as plain cement paste. Under this Level 2 approximation, the D-EMT calculations were actually quite accurate with respect to the experimental data. The accuracy of the D-EMT was then further improved by considering that the amount and distribution of hydration products in the ITZ, i.e., the extra CH in the ITZ, can increase its elastic moduli compared to a plain cement paste of the same w/c ratio and degree of hydration. This CH redistribution has been seen experimentally [2,3] but for the first time its effect on elastic moduli has been computed, albeit within the assumptions of the VCCTL hydration module. This redistribution also occurs for other phases like ettringite. The small amounts of these phases along with their elastic moduli, which are smaller than those of CH, combine to make their redistribution only a minor effect.

The accuracy of the D-EMT is closely related to the elastic moduli contrast between the effective particle inclusions and the bulk paste matrix. In general, smaller contrasts, caused by stiffer paste matrices, lead to smaller relative errors between D-EMT and experiment.

It would be straightforward, in future research, to consider the entrained air content as a fourth phase in the modeling and simulation [4]. These inclusions would have zero elastic moduli but with an ITZ surrounding them [73]. It would also be interesting but difficult to develop the D-EMT for real, random-shape aggregate particles. A non-spherical geometry makes the effective inclusion problem much more complicated. Randomly shaped aggregates would probably not make much difference at later ages, but might be very important at early ages, where the contrast between aggregates and cement paste can be very high, a case where the effect of inclusion shape on composite elastic moduli can be significant [34–37].

Acknowledgements

The research presented in the paper was partially funded by the Infrastructure Technology Institute at Northwestern University, the Center for Advanced Cement-Based Materials at Northwestern University, the National Science Foundation (Grant No. 0408427), the Federal Highway Administration (Grant No. DTFH61-05-C-0001), and the University of Louisville. Their financial support is gratefully acknowledged. We also thank the HYPERCON program at NIST and the Virtual Cement and Concrete Testing Laboratory for partial support of this research.

References

- [1] Scrivener KL. The microstructure of concrete. In: Skalny J, editor. *Material science of concrete*, vol. 1. Westerville, OH: American Ceramic Society; 1989. p. 127–62.
- [2] Scrivener KL, Pratt PL. Characterization of interfacial microstructure. In: Maso JC, editor. *Interfacial transition zone in concrete*, RILEM Report 11, E&FN Spon, London, 1996. p. 3–17.
- [3] Scrivener KL. Characterization of the ITZ and its quantification by test methods. In: Alexander MG, Arliguie G, Ballivy G, Bentur A, Marchand J, editors. *Engineering and transport properties of the interfacial transition zone in cementitious composites*, RILEM Report 20, RILEM Publications S.A.R.L., France, 1999. p. 3–15.
- [4] Scrivener KL, Nemat KM. The percolation of pore space in the cement paste/aggregate interfacial zone of concrete. *Cem Conc Res* 1996;26(1):35–40.
- [5] Bentz DP, Garboczi EJ, Stutzman PE. Computer modeling of the interfacial transition zone in concrete. In: Maso JC, editor. *Interfaces in cementitious composites*. London: E. and F.N. Spon; 1993. p. 259–68. Available from: <http://ciks.cbt.nist.gov/monograph>, Part I, Chapter 6. Section 3.
- [6] Bentz DP, Stutzman PA, Garboczi EJ. Experimental and simulation studies of the interfacial zone in concrete. *Cem Conc Res* 1992;22(5): 891–902.
- [7] Scrivener KL, Gariner EM. Microstructural gradients in cement paste around aggregate particles. In: Mindess S, Shah SP, editors. *Bonding in cementitious composites*. Mater Res Soc Symp Proc, vol. 114. p. 77–85.
- [8] Prokopski G, Halbiniaik J. Interfacial transition zone in cementitious materials. *Cem Conc Res* 2000;30(4):579–83.
- [9] Liao KY, Chang PK, Peng YN, Yang CC. A study on characteristics of interfacial transition zone in concrete. *Cem. Conc. Res.* 2004;34(6): 977–89.
- [10] Garboczi EJ, Bentz DP, Schwartz LM. Modeling the influence of the interfacial zone on the D.C. electrical conductivity of mortar. *Adv. Cement-Based Mater.* 1995;2(5):169–81.
- [11] Brandt AM. *Cement-based composites: materials, mechanical properties and performance*. London, UK: E&FN Spon; 1995.
- [12] Simeonov P, Ahmad S. Effect of transition zone on the elastic behavior of cement-based composites. *Cem Conc Res* 1995;25(1): 165–76.
- [13] Nilsen AU, Monteiro PJM. Concrete: a three-phase material. *Cem Conc Res* 1993;23(1):147–51.
- [14] Yang CC. Effect of the transition zone on the elastic moduli of mortar. *Cem Conc Res* 1998;28(5):727–36.
- [15] Yang CC. Effect of the interfacial transition zone on the transport and the elastic properties of mortar. *Mag Conc Res* 2003;55(4): 305–12.
- [16] Li CQ, Zheng JJ, Zhou XA, McCarthy MJ. A numerical method for the prediction of elastic modulus of concrete. *Mag Conc Res* 2003; 55(6):497–505.

- [17] Li G, Zhao Y, Pang SS. Four-phase modeling of effective bulk modulus of concrete. *Cem Conc Res* 1999;29(6):839–45.
- [18] Li G, Zhao Y, Pang SS, Li Y. Effective Young's modulus of concrete. *Cem Conc Res* 1999;29(9):1455–62.
- [19] Winslow N, Cohen MD, Bentz DP, Snyder KA, Garboczi EJ. Percolation and porosity in mortars and concretes. *Cem Conc Res* 1994;24(1):25–37.
- [20] Garboczi EJ, Berryman JG. New effective medium theory for the diffusivity or conductivity of a multi-scale concrete microstructure model. *Conc Sci Eng* 2000;2(6):88–96.
- [21] Garboczi EJ, Berryman JG. Elastic moduli of a material containing composite inclusions: effective medium theory and finite element computations. *Mech Mater* 2001;33:455–70.
- [22] Bentz DP, Garboczi EJ, Snyder KA. A hard core/soft shell microstructural model for studying percolation and transport in three-dimensional composite media, NIST Internal Report 6265, 1999.
- [23] Christensen RM, Lo KH. Solutions for effective shear properties on three phase sphere and cylinder models. *J Mech Phys Solids* 1979; 27(4):315–30.
- [24] Garboczi EJ, Day AR. An algorithm for computing the effective linear elastic properties of heterogeneous materials: three-dimensional results for composites with equal phase Poisson ratios. *J Mech Phys Solids* 1995;43(9):1349–62.
- [25] Nadeau JC. Water–cement ratio gradients in mortars and corresponding effective elastic properties. *Cem Conc Res* 2002;32(3): 481–90.
- [26] Nadeau JC. A multi-scale model for effective moduli of concrete incorporating ITZ water–cement ratio gradients in mortars, aggregate size distributions, and entrapped voids. *Cem Conc Res* 2003;33(1): 103–13.
- [27] Sun, Z. Monitoring the early-age properties of cementitious materials with ultrasonic wave reflection method at macro- and micro-structural levels. PhD thesis, Northwestern University, 2005.
- [28] McLaughlin R. A study of the differential scheme for composite materials. *Int J Eng Sci* 1977;15(4):237–44.
- [29] Norris AN. A differential scheme for the effective moduli of composites. *Mech Mater* 1985;4(1):1–16.
- [30] Bentz DP, Garboczi EJ, Lagergren ES. Multi-scale microstructural modelling of concrete diffusivity: identification of significant variables. *Cem Conc Res* 1998;20(1):129–39.
- [31] Garboczi EJ, Bentz DP. Analytical formulas for interfacial transition zone properties. *Adv Cement-Based Mater* 1997;6(3–4):99–108.
- [32] Garboczi EJ, Bentz DP. Multi-scale analytical/numerical theory of the diffusivity of concrete. *Adv Cement-Based Mater* 1999;8(2):77–88.
- [33] Shane JD, Mason TO, Jennings HM, Garboczi EJ, Bentz DP. Effect of the interfacial transition zone on the conductivity of portland cement mortars. *J Am Ceram Soc* 2000;83(5):1137–44.
- [34] Douglas JF, Garboczi EJ. Intrinsic viscosity and polarizability of particles having a wide range of shapes. *Adv Chem Phys* 1995;91: 85–153.
- [35] Garboczi EJ, Douglas JF. Intrinsic conductivity of objects having arbitrary shape and conductivity. *Phys Rev E* 1996;53(6):6169–80.
- [36] Mansfield ML, Douglas JF, Garboczi EJ. Intrinsic viscosity and the electrical polarizability of arbitrarily shaped objects. *Phys Rev E* 2001;64:61401–16.
- [37] Garboczi EJ, Douglas JF, Bohn RB. A hybrid finite element-analytical method for determining the intrinsic elastic moduli of particles having moderately extended shapes and a wide range of elastic properties. *Mech Mater* 2006;38(8–10):786–800.
- [38] Herve E, Zaoui A. N-Layered inclusion-based micromechanical modelling. *Int J Eng Sci* 1993;31(1):1–10.
- [39] Iske PL, Sterk NKJ, Oortwijn J. Effective elastic properties of suspensions of radially symmetric particles. *Physica A* 1994;209(1–2): 96–128.
- [40] Lutz MP, Monteiro PJM. Effect of the transition zone on the bulk modulus of concrete. In: Diamond S, Mindess S, Glasser FP, Roberts LW, Skalny JP, Wakeley LD, editors. *Microstructure of cement-based systems/bonding and interfaces in cementitious materials*, vol. 370. Pittsburgh: Materials Research Society; 1995.
- [41] Lutz MP, Monteiro PJM, Zimmerman RW. Inhomogeneous interfacial transition zone model for the bulk modulus of mortar. *Cem Conc Res* 1997;27(7):1113–22.
- [42] Stutzman P. Scanning electron microscopy imaging of hydraulic cement microstructure. *Cem Conc Comp* 2004;26(8):957–66.
- [43] Rawle A. Basic principles of particle size analysis. Malvern Instruments. Available from: www.malvern.co.uk.
- [44] ASTM C33-99a, Standard specification for concrete aggregates.
- [45] ASTM C305-82, Standard practice for mechanical mixing of hydraulic cement pastes and mortars of plastic consistency.
- [46] ASTM C192-88, Standard practice for making and curing concrete test specimens in the laboratory.
- [47] ASTM C191-99, Standard test method for time of setting of hydraulic cement by Vicat needle.
- [48] ASTM C215-97, Standard test method for fundamental transverse, longitudinal, and torsional resonant frequencies of concrete specimens.
- [49] Powers TC. The Nonevaporable water content of hardened portland-cement paste—its significance for concrete research and its method of determination. *ASTM Bulletin* 1949;158:68–76.
- [50] Copeland LE, Hayes JC. The determination of non-evaporable water in hardened portland cement pastes. *ASTM Bull* 1953;194:70–4.
- [51] Macrae JC, Gray WA. Significance of the properties of materials in packing of real spherical particles. *Brit J Appl Phys* 1961;12(4): 164–72.
- [52] Lu B, Torquato S. Nearest surface distribution functions for polydispersed particle systems. *Phys Rev A* 1992;45(8):5530–44.
- [53] Bentz DP. Three-dimensional computer simulation of portland cement hydration and microstructure development. *J Am Ceram Soc* 1997;80(1):3–21.
- [54] Bentz DP. CEMHYD3D: A three-dimensional cement hydration and microstructure development modeling package: version 3.0, National Institute of Standards and Technology Interagency Report, US Department of Commerce, NISTIR 7232, June 2005. Available as Appendix I-2 of the Electronic Monograph at <http://ciks.cbt.nist.gov/monograph>. Software available at <ftp://ftp.nist.gov/pub/bfrl/bentz/CEMHYD3D/version30/>.
- [55] Garboczi EJ, Bullard JW, Bentz DP. Status of virtual testing of cement and concrete in the US – 2004. *Conc Int* 2004;26(12):33–7.
- [56] Garboczi EJ, Bentz DP. The effect of statistical fluctuation, finite size error, and digital resolution on the phase percolation and transport aspects of the NIST cement hydration model. *Cem Conc Res* 2001; 31(10):1501–14.
- [57] Garboczi EJ, Bullard JW. Shape analysis of a reference cement. *Cem Conc Res* 2000;34(10):1933–7.
- [58] Bullard JW, Garboczi EJ. A model investigation of the influence of particle shape on portland cement hydration. *Cem Conc Res* 2006; 36(6):1007–15.
- [59] Constantinides G, Ulm FJ. The effect of two types of C–S–H on the elasticity of cement-based materials: results from nanoindentation and micromechanical modeling. *Cem Conc Res* 2004;34(1):67–80.
- [60] Ramesh G, Sotolino ED, Chen WF. Effect of transition zone on elastic moduli of concrete materials. *Cem Conc Res* 1996;26(4): 611–22.
- [61] Haecker CJ, Garboczi EJ, Bohn RB, Sun Z, Voigt T, Shah SP. Modeling the linear elastic properties of cement paste. *Cem Conc Res* 2005;35(10):1948–60.
- [62] Taplin JH. A method for following the hydration reaction in portland cement paste. *Aust J Appl Sci* 1959;10:329–45.
- [63] Yudenfreund M, Odler I, Brunauer S. Hardened portland cement pastes of low porosity I. materials and experimental methods. *Cem Conc Res* 1972;2(3):313–30.
- [64] Knudsen T. The dispersion model for hydration of portland cement I. General concepts. *Cem Conc Res* 1984;14(5):622–30.
- [65] Carino NJ. The maturity method: theory and application. *Cem Conc Res* 1984;2(2):61–73.

- [66] Sun Z, Ye G, Shah SP. Microstructure and early-age properties of Portland cement pastes – effects of the connectivity of the solid phases. *ACI Mater J* 2005;102(2):122–9.
- [67] Garboczi EJ. Finite element and finite difference programs for computing the linear elastic and elastic properties of digital images of random materials, NIST Internal Report 6269, 1998. Also available at <http://ciks.cbt.nist.gov/monograph/>, Part III, Chapter 2.
- [68] Bohn RB, Garboczi EJ. User manual for finite element and finite difference programs: a parallel version of NIST IR 6269, NIST Internal Report 6997, 2003.
- [69] Monteiro PJM, Chang CT. The elastic moduli of calcium hydroxide. *Cem Conc Res* 1995;25(8):1605–9.
- [70] Berryman JG. Bounds and self-consistent estimates for elastic constants of random polycrystals with hexagonal, trigonal, and tetragonal symmetries. *J Mech Phys Sol* 2005;53(10):2141–73, and references herein.
- [71] Tasong WA, Lynsdale CJ, Cripps JC. Aggregate-cement paste interface part I: influence of aggregate geochemistry. *Cem Conc Res* 1999;29(7):1019–25.
- [72] Sample program is located at <ftp.nist.gov/pub/bfrl/garbocz/ITZ-SUN/DEMT.f> (Fortran 77).
- [73] Rashed AI, Williamson RB. Microstructure of entrained air voids in concrete I. *J Mater Res* 1991;6:2004–12; Rashed AI, Williamson RB. Microstructure of entrained air voids in concrete II 1991;6:2474–83.